Vacuum 165 (2019) 337–342

Contents lists available at ScienceDirect

Vacuum

journal homepage: www.elsevier.com/locate/vacuum

Comparative numerical study of the dynamics, ion beam and flow energetics of fast and slow focus modes in a 2 kJ plasma focus operated in various gases

S.H. Saw[a,d,e], V. Damideh[b,*], O.H. Chin[b], J. Ali[c], P.C.K. Lee[d], R.S. Rawat[d], S. Lee[a,b,e]

[a] Institute for Plasma Focus Studies, Chadstone, Vic.3148, Australia
[b] Plasma Technology Research Centre, Department of Physics, University of Malaya, 50603, Kuala Lumpur, Malaysia
[c] Laser Center, Ibnu Sina ISIR, Physics Department, Universiti Teknologi Malaysia, 81310, Johor Bahru Malaysia, Malaysia
[d] Radiation Sources Laboratory, Natural Sciences and Science Education, National Institute of Education, Nanyang Technological University, 637616, Singapore
[e] INTI International University, Nilai, 71800, Malaysia

ARTICLE INFO

Keywords:
Plasma focus
Slow focus mode
Ion beam
Plasma stream
Fusion first wall materials
Nano-phase materials
Lee model code

ABSTRACT

Comparative study of fast focus mode (FFM) and slow focus mode (SFM) of INTI Plasma Focus device at 12 kV, based on Lee Model, are presented in this paper. Results of numerical experiments for D, Ne, and Ar gases at different pressure ranges show that as a rule-of-thumb, diameter-optimized SFM is considered to occur when fast plasma stream speed generated by pinch column is equal to the peak axial phase speed. SFM occurs at the high-pressure range of operation when beam ion energy is typically less than a few keV. Results of speed factor, fast ion beam energy, FPS energy, FIB damage factor, plasma footprint radius for FFM and SFM at different pressures of D, Ne, and Ar are presented. These results may be used to predict different applications of both modes: for example, the intense beam and flow energetics in FFM may be of interest in irradiation of surfaces for damage studies; whilst in SFM, the larger area of reduced intensity of plasma flow and very low energy per beam ion result in more uniform irradiation over a larger area of target. This larger more uniform area of irradiation has distinct advantages in nanophase material synthesis by diameter-optimized SFM.

1. Introduction

Dense Plasma Focus (PF) device can produce directed hot (1 keV) fast (10^7 cm/s) dense (10^{16} - 10^{19} cm^{-3}) plasma streams, fast ion beam (0.01–100 MeV), electron beam (0.01–1 MeV), soft (0.1–10 keV) and hard (10–1000 keV) X rays and fusion neutrons (2.45 and 14 MeV). These PF devices are used for irradiating different materials to pulsed beams of various types; ion, electron, X-radiation, neutron, high power plasma streams and shock waves [1–5].

Pulsed plasmas at high temperatures and densities are produced in these PF devices [6,7]. Future reactors will use the fusion reaction D + T → n (14.1 MeV) + ^{4}He (3.5 MeV) for power production. Radiations of neutrons together with alpha particles and heavy ions from the walls of the plasma chamber will be prone to cause damage to exposed surfaces. PF devices operated in conventional energy optimized 'fast' mode are sources of similar intense radiation and hence are suitable to study the behavior of materials under such intense fusion-related radiation. Specifically, tungsten, and other prospective plasma-facing materials may be tested with PF devices [1,8].

On the other hand, nano-materials fabrication and production are also important applications of PF devices [9]. For such purposes the radiations and beams need to be controlled. The intensities have to be reduced and for some applications the pinch phase may be required to be so much softened that practically this final sub-phase of compression may even to be eliminated [1,9]. Such a controlled softening of plasma focus conditions has led to the idea of the Slow Focus Mode (SFM) [10,11]. The ZaP flow z-pinch using essentially much softer plasma flows than in conventional z-pinches has similarly attempted to demonstrate effectiveness in an area of material application [12].

The aim of this paper is to investigate the Fast Focus Mode (FFM) and Slow Focus Mode (SFM) of INTI PF and compare their properties with an aim to improve their performance for material science applications. In this research we will highlight the contrast in conventional use of PF's (i) to produce intense ion beam and streaming plasma pulses from FFM, with the controlled production of (ii) high power long duration uniform flow of plasma ions and streaming plasma pulses from SFM. This contrast is vividly demonstrated using Lee Model Code at different pressures of D, Ne, and Ar gases.

* Corresponding author.
E-mail address: v_damideh@yahoo.com (V. Damideh).

https://doi.org/10.1016/j.vacuum.2019.04.042
Received 17 January 2019; Received in revised form 17 April 2019; Accepted 18 April 2019
Available online 23 April 2019
0042-207X/ © 2019 Elsevier Ltd. All rights reserved.

2. Numerical experiments

Physical Simulation helps to improve the understanding of the phenomena. When applied to the development of manufacturing process simulation can guide the direction of the process, increase precision and can improve efficiency and lower the cost of the process. Numerical simulation has become an important method for process study, design, construction and optimization. By using numerical experiments, a process can be modeled and optimized for better performance. In the case of PF devices there are a variety of modeling methods [13–17]. A pre-1995 version of Lee Model Code omitted the crucial element of 'communication delay' between the driven shock front and the driving magnetic force [18,19]. This omission was remedied after 1995 [20,21]. The post- 1995 version has an acceptable correlation with experimental results especially in terms of dynamics and radiation yields.

The axial phase adopts the snow-plow model whilst the radial inward shock phase uses the slug model with thermodynamics [22–24]. The pinch phase is radiation-coupled. Circuit equations are rigorously coupled with the dynamics so that the code is mass, energy and charge consistent. The code uses mass swept-up and effective current factors f_m, f_c, (for axial phase) and f_{mr}, and f_{cr} (for radial phase). These model parameters are experimentally measured by fitting computed current traces with those obtained in laboratory experiments. Insights including optimum static inductance and current and neutron scaling and saturation have resulted [25,26]. The pinch phase incorporates radiation-coupled motion resulting in computation of radiative-collapse in the PF pinch [27]. Computations of Soft X-ray (SXR) have been validated by measurements in INTI PF [28] with Ne. This has led to optimization of the INTI PF for Ne SXR production [29].

The code computes both beam-target and thermonuclear components of fusion neutrons and has generated neutron scaling laws [30,31]. Likewise scaling laws for SXR and ions are obtained in terms of, total current, pinch current and stored energy [31–33].

Fast ion beam (FIB) and fast plasma stream (FPS) are computed [34]. A fast plasma stream (FPS) is associated with the post pinch processes [29]. The code computes the energy of the FPS. Recently interferometric studies of PF-400 J are published with estimates of FIB and FPS properties [35]. These measured values are validating the computed values from our code [36]. Specifically, computed power flow density (energy flux) and damage factor are 2.45×10^{12} W m^{-2} (twice the published experimental value) and 1.78×10^{8} Wm^{-2} s$^{0.5}$ (almost the same as published experimental value) respectively [36]. Moreover, a recent search has compiled further verification of computed versus measured beam current densities from a 2.3 kJ PF and a 2.2 kJ [37–39].

The above verification of the estimates of ion beam numbers and properties gives confidence for these quantities to be computed for the present project to study the comparative performance of INTI PF in FFM and SFM.

INTI PF has 0.95 radius copper hollow anode with length of 16 cm. The 3.2 cm radius cathode is formed of six copper bars surrounding the anode. It stores 3 kJ in a single fast 30 μF capacitor when operated at 15 kV. The static inductance of the discharge circuit is 120 nH. At 12 kV, INTI PF operates in its time-matched FFM at relatively low pressures of filling gas; for example, 3 Torr of D. (By time-matched we mean that the radial phase starts at or not too far below peak current). Then, by suitably increasing the filling gas pressure it operates in SFM.

Previous studies have shown that in a low energy PF device, and even across two PF devices of similar energies, the model parameters f_m, f_c, f_{mr}, and f_{cr} may be considered to be almost constant over a range of pressures [40]. This enables us to fix earlier fitted values of the model parameters for the INTI PF, which we show in Table 1 which also shows values of tube, model and operational parameters together with static inductance of 120 nH and circuit stray resistance of 12 mΩ.

In the following section we show and discuss the results. Figs. 1–9 show the results for the pressure range of 1–14 Torr D, 1–5.5 Torr Ne, and 0.2–2.4 Torr Ar. From the results, we conclude that the time-matched pinch for INTI PF at 12 kV for D, Ne, and Ar occurs at 3 Torr, 2 Torr, and 1 Torr respectively. From the results, we select 3 Torr D, 2 Torr Ne, and 1 Torr Ar for FFM operation of INTI PF machine and 14 Torr D, 5.5 torr Ne, and 2.4 Torr Ar for diameter-optimized SFM operation.

Table 1
Tube, model and operation parameters of INTI PF.

Tube Parameters					
L_0 (nH)	C_0 (uF)	b (cm)	a (c)	z_0 (cm)	r_0 (mΩ)
120	30	3.2	0.95	16	12

Model Parameters				
Gas	Mass factor f_m	Current factor f_c	Radial mass factor f_{mr}	Radial current factor f_{cr}
D	0.08	0.7	0.16	0.7
Ne	0.04	0.7	0.2	0.7
Ar	0.05	0.7	0.2	0.7

Operational Parameters					
Gas	Vo (kV)	Po (Torr)	MW	A	At-1 mol-2
D	12	3	4	1	2
Ne	12	2	20	10	1
Ar	12	1	40	18	1

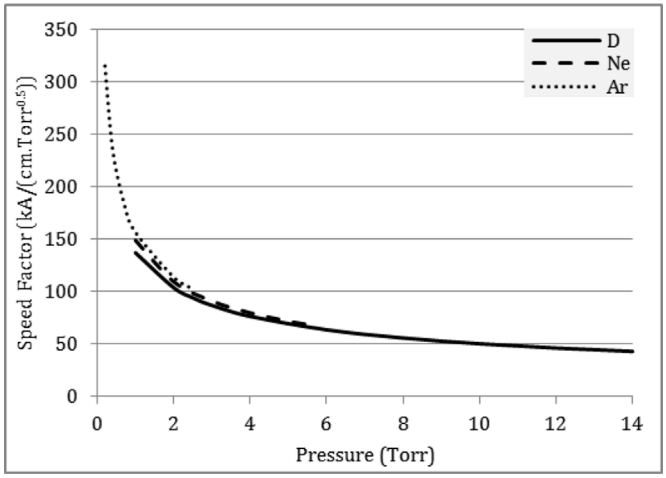

Fig. 1. Speed factor versus pressure in INTI PF.

3. Results and discussion

The speed factor S (current per unit anode radius divided by square root of density) in an electromagnetic device [41] is a measure of the plasma speed in the device. Replacing the dependence on density as a dependence on pressure separates the range of S on the scale of useable pressure for D, Ne, and Ar. Fig. 1 shows that by increasing the pressure in INTI PF, the value of S decreases from 137 kA/(cm$\sqrt{\text{Torr}}$)at 1 Torr D (FFM but too fast for time-matching since the radial phase starts long before the discharge current peaks) to 43 kA/(cm$\sqrt{\text{Torr}}$) at 14 Torr (SFM). This covers the useable range of INTI PF operated in D. For Ne, the value of S at FFM of at 2 Torr is 109 kA/(cm$\sqrt{\text{Torr}}$) and for its SFM operation at 5.5 Torr is 69 kA/(cm$\sqrt{\text{Torr}}$). Also speed factor of Ar drops from 156 kA/(cm$\sqrt{\text{Torr}}$) for 1 Torr FFM to 104 kA/(cm$\sqrt{\text{Torr}}$) for 2.4 Torr for SFM.

The final size of the pinch column at the end of the pinch phase, for

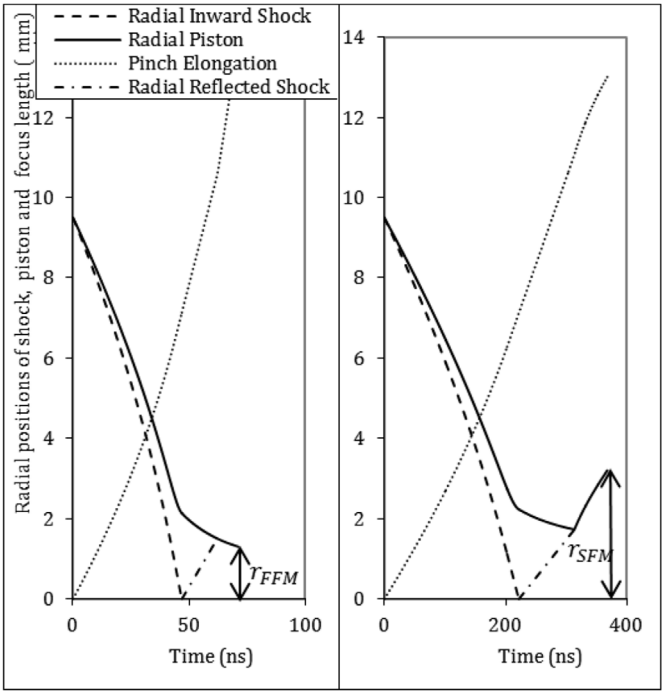

Fig. 2. Presents the computed radius versus time (r–t), graph depicting the radial trajectories of the inward-moving shock and piston when operated in D. When the inward shocked plasma stagnates on the axis of symmetry, a reflected shock (RS) moves outwards, its trajectory is also shown in Fig. 2. The computation follows the RS shock outwards until it hits the inward-moving piston, whereupon the trajectory of the pinch is also presented. The pinch trajectory is computed until its end, the duration being determined by the transit time of small disturbance speed across the radial dimension of the pinch. The LHS of Fig. 2 shows that at 3 Torr D the RS hits the piston decisively, but the piston is compressing inwards strongly driven by the current at or near its peak value. Thus, a strongly compressing pinch results with the radius of the pinch reducing until it reaches its maximum compression at minimum radius. The RHS of Fig. 2 shows the situation at 14 Torr D. Note that the piston trajectory is slowing down and is approaching a zero slope when it is hit by the RS. Because of the high pressure and the slow axial speed, the radial phase is reached when the current has already peaked and dropped to less than half the peak value. Thus, the piston is only weakly compressing. The RS pushes the weak piston outwards and at the end of the pinch phase the pinch has a large diameter. When the pressure is increased beyond 14 Torr, the trajectory of the piston turns upwards so much that the RS does not reliably catch up with the piston. Hence, we consider that beyond 14 Torr no reliable pinch occurs; and 14 Torr D is taken as the diameter-optimized SFM.

this diameter-optimized (case when the diameter of the pinch is at maximum value) SFM is shown as r_{SFM} in Fig. 2; and is considered as the plasma stream exit radius. In the case of D operated in SFM, the plasma stream has a cross sectional area "A_{SFM}" at pinch exit 6 times more than for FFM "A_{FFM}":

$$\frac{A_{SFM}}{A_{FFM}} = \frac{r_{SFM}}{r_{FFM}} = \left(\frac{3.18}{1.31}\right)^2 \approx 6$$

In the case of Ne "A_{SFM}" is 18 times more "A_{FFM}".

In the case of Ar, in optimized FFM the pinch compresses to very small radius due to radiative collapse, resulting in area enhancement of more than 200 times [24]. The maximum diameter of pinch exit for Ar for SFM is computed as 11.6 mm. The bigger pinch exit diameter is important for deposition applications. The comparable values for Ne and D are both just over 6 mm. Fig. 3 shows the pinch exit radius as a function of pressure.

Computed values of average FIB energy (per ion) for D, Ne, and Ar versus filling gas pressure in INTI PF are presented in Fig. 4. During optimized FFM operation, average FIB energy per ion for D and Ne are

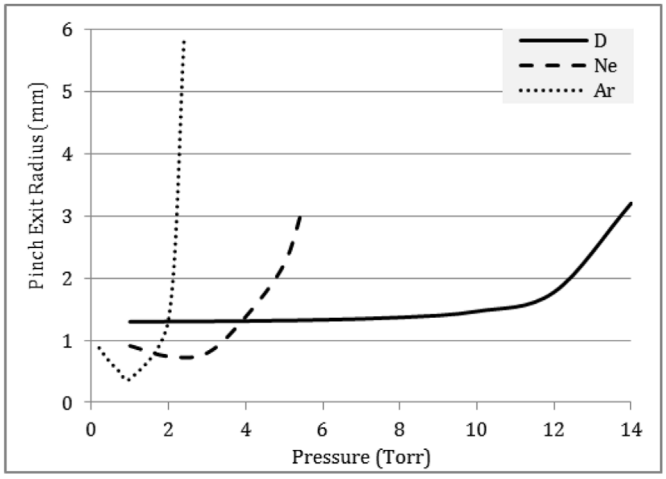

Fig. 3. The radius of pinch exit in INTI PF for D, Ne, and Ar. Fig. 2. Computed radial trajectories of INTI PF based on Lee Model Code for 3 Torr D(left) and 14 Torr D(right); FFM (left), SFM (right).

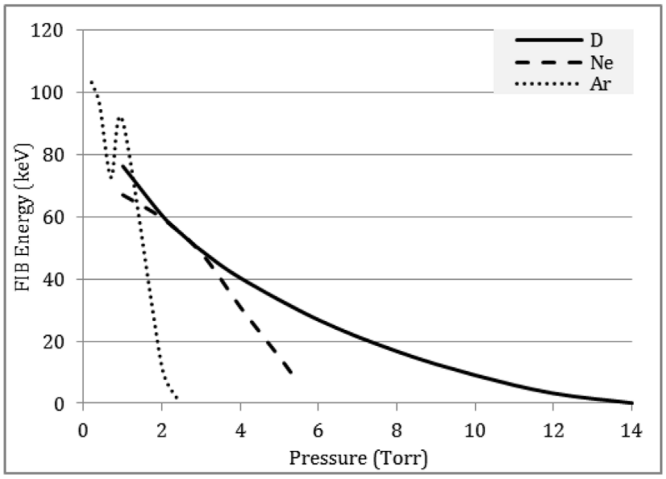

Fig. 4. Fast ion beam energy (per ion) versus D, Ne, and Ar pressure in INTI PF based on Lee Model Code.

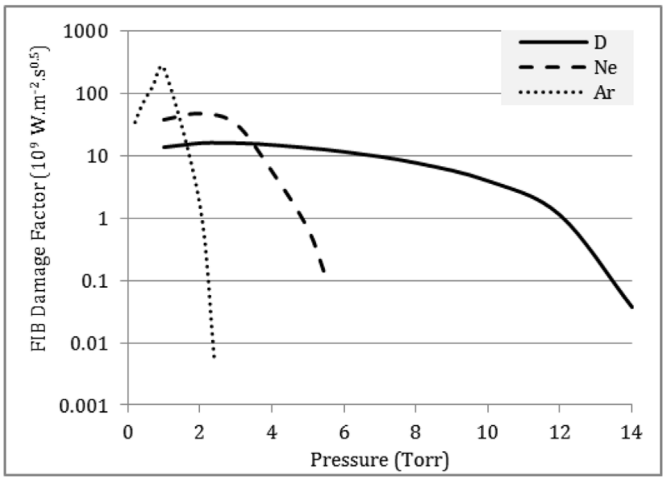

Fig. 5. FIB damage factor for D, Ne, and Ar in INTI PF.

49 keV and 60 keV respectively while for SFM operation their values are 0.17 keV and 6 keV, respectively. Thus, average FIB energy per ion for D and Ne during SFM are 285 and 10 times lower than for FFM

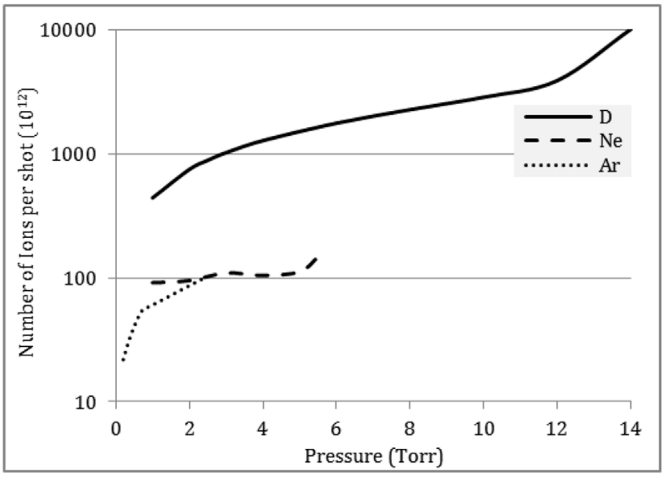

Fig. 6. Number of ions per shot in INTI PF versus D, Ne, and Ar pressure based on Lee Model Code.

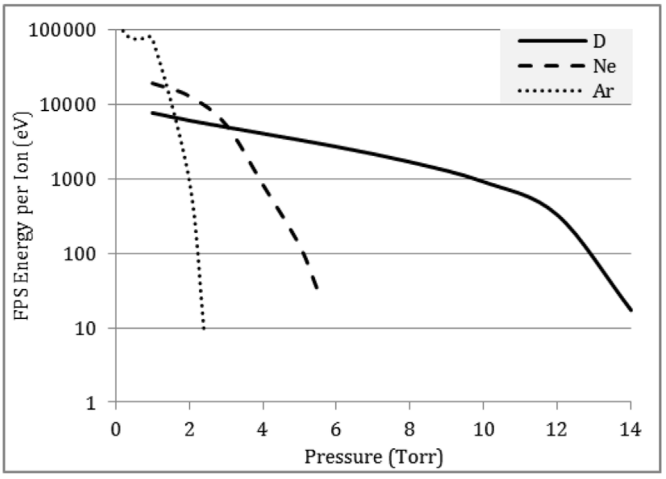

Fig. 7. FPS energy per ion in INTI PF for D, Ne, and Ar.

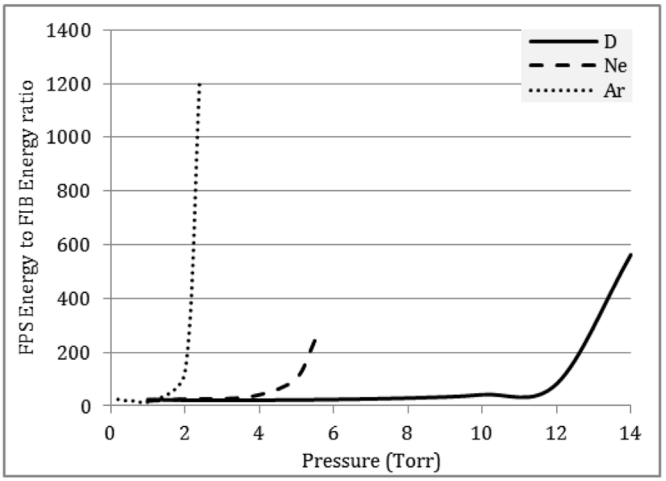

Fig. 8. FPS energy to FIB energy ratio in INTI PF for D, Ne, and Ar.

operation. These values for Ar are 91 keV and 1 keV respectively for FFM and SFM operations; i.e. the average FIB energy for SFM is 91 times lower than for FFM.

Decrease in average FIB energy per ion leads to decrease in FIB damage factor in INTI PF. Fig. 5 shows damage factor versus

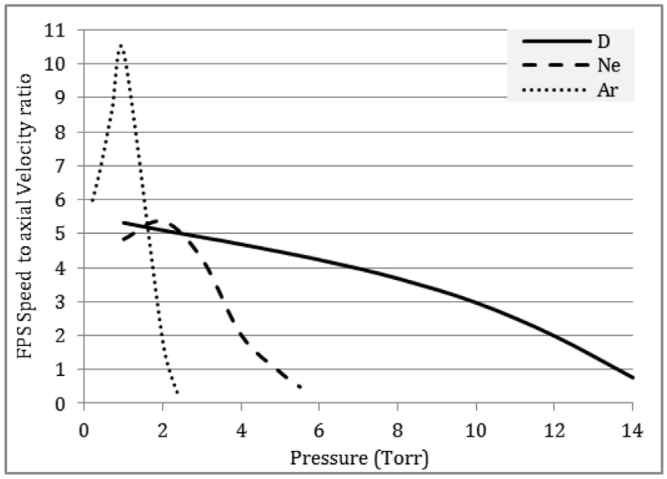

Fig. 9. FPS speed to axial velocity ratio in INTI PF for D, Ne, and Ar.

operational pressure in D, Ne, and Ar. As seen in Fig. 5 the maximum damage factor, are in FFM operation at about 3 Torr, 2 Torr and 1 Torr respectively for D, Ne, and Ar. Damage factors of FFM operation using D, Ne, and Ar are 423, 427 and 4700 times higher than their values during SFM operation.

Computed numbers of ions per shot in INTI PF for D, Ne and Ar versus gas pressure, show that the highest ion production is at the highest gas pressure we operated in the case of D (14 Torr), Ne (5.5 Torr) and Ar (2.4 Torr). As mentioned earlier, SFM operation produces much higher number of ions than FFM operation as seen in Fig. 6.

Our computation shows that FPS energy (total energy of FPS) of SFM for D, Ne, and Ar is only slightly lower than that in FFM. However, the SFM FPS energy per ion for D and Ne (Fig. 7) are 285 and 400 times lower than for FFM in INTI PF. Also, SFM FPS energy per ion for Ar is 8200 times lower than for FFM. Thus, the energy of each FPS ion is not so high as to be damaging (but high enough for beneficial materials interaction); yet the total energy the FPS ions carry for target interaction in SFM is almost as high as in FFM.

As shown in Fig. 8, the ratio of FPS energy to FIB energy; per ion, in the case of SFM is so much higher than that of FFM for D, Ne, and Ar in INTI PF. In SFM the FPS for INTI PF working in D, is 560 times that of FIB while in FFM the same comparison is 20 times. For Ne this ratio is 246 and 26 for SFM and FFM respectively. Also, for Ar, this ratio for SFM operation at 2.4 Torr is 1222 and about 15 for FFM.

The FPS speed to axial velocity ratio versus pressure is shown in Fig. 9. It appears that the diameter-optimized SFM occurs for each of the three gases when this ratio has a value just below 1. As a convenient rule-of-thumb we may consider that diameter-optimized SFM occurs when the FPS speed is equal to plasma axial velocity at the end of axial phase. This is the highest pressure at which the focus pinch still occurs. It may also be considered as the operating pressure of slowest SFM. At any higher pressures the reflected shock does not reach the piston and the PF device operates as an electromagnetic shock tube with no pinch effect. As a rule-of-thumb, the biggest plasma footprint area with post-pinch FPS may be considered to be achieved when the ratio of the FPS speed to axial velocity is equal to 1.

In summary, the computations show that INTI PF is suitable for nano-material synthesis and material deposition using the SFM operation because of following reasons:

- Average FIB energy per ion for SFM is much lower than for FFM; resulting in lower damage factor
- Damage factor for SFM is much lower (10^8 and lower) than for FFM
- Plasma footprint area for SFM is much bigger than for FFM
- The ratio of FPS energy to FIB energy for SFM is higher than for FFM
- FPS energy per ion for SFM is much lower than for FFM; yet high

enough for interaction with targets for fabrication purposes
- Low ion current density, bigger plasma footprint area and higher number of ions per shot accompanied by equal FPS and axial speed for SFM can produce more uniform plasma stream than for FFM.

The above points appear advantageous for materials deposition and seem consistent with observations made in irradiation experiments on tungsten and graphite targets (see concluding paragraph of Section 4 Conclusions).

Moreover, the plasma focus has been proposed for fusion first wall material investigations using the FFM operation which is the normal intense mode of operation of PF. This has been claimed for the cases of several PF devices ranging from the big PF1000 to several small PF devices [1–5,9,10,41,42]. INTI PF belongs within this range of devices particularly in terms of constancy of fluence and flux, energy fluence and energy flux and damage factor across the range of devices [32,34]. The constancy of damage factor across the range of PF devices essentially means that all properly optimized PF devices are suitable for fusion first wall investigations, the difference being in the size of test target samples. The bigger devices are suitable for testing bigger target samples whilst the smaller devices are limited to smaller target samples. Specifically, for the INTI PF the following are shown by our computation:

- Average FIB energy per ion for FFM is higher than for SFM
- Damage factor for FFM is so much higher (10^{10} and greater) than for SFM
- FPS energy per ion for FFM is higher than for SFM
- High ion current and current density, smaller plasma footprint area accompanied by higher energy ions of FFM can make more effective damages on material surfaces than SFM.

4. Conclusion

Numerical experiments based on Lee Model Code using different pressures of D, Ne, and Ar show that INTI PF in its FFM operation may be suitable for material investigations from the point of view of high ion current and current density, high energy ions and high damage factor (greater than 10^{10}). On the other hand, operating in pinch diameter-optimized SFM, the average FIB energy, average FPS energy per ion and damage factor for SFM is much lower than for FFM while energy into plasma and number of ions per shot for SFM is higher than for FFM. Moreover, the ratio of FPS energy to FIB energy for SFM is higher than for FFM. The low ion current density, higher number of ions per shot and bigger plasma footprint area in diameter-optimized SFM could make INTI PF more suitable for nano-material synthesis and material deposition. It is expected that such diameter-optimized SFM regimes could be defined for other plasma focus machines also in addition to their usual FFM regimes.

With regards to experimental verification of the SFM and FFM, we note the following results which are published [43,44]. As the pressure is increased, the focus pinch occurs progressively at later times and lower currents. The focus pinch intensity (as shown from focus voltage spike) decreases until at sufficiently high pressure, all indications of the focus pinch has disappeared. Clearly at high enough pressures, the device no longer pinches. The SFM occurs near the highest pressure when the focus spike (with corresponding indications on the rate of change of current measurement) is still present, both experimentally and in computations. We have confirmed the agreement between computations and measurements in this respect. Since the FIB is caused by the inductive and or anomalous resistive voltages of focus pinch, all experimental evidence and concurring computational results indicates that the energy per beam ion is reduced for the higher pressure SFM. Thus, for SFM operation whilst still producing a good energetic plasma streams FPS, the FIB is no longer damaging, and the interactions with target in SFM is mainly through the FPS.

Preliminary exposures of targets to the radiations and plasmas from the INTI PF have also been made at different pressures and distances from the focus pinch. At 12 kV, 2.5 Torr D, a tungsten target facing the focus pinch at a distance of 4 cm (ie four anode radius), we identified from marks on the target that the FIB had a footprint of just under 2 mm (not limited by a double aperture placed between the pinch and the target); whilst the FPS has a footprint of more than 4 mm being limited by the double aperture. As the pressure was increased to 12 Torr D, there was no central mark made by the FIB and the FPS footprint had increased to more than 12 mm. These results are consistent with our computational findings of SFM operation of a larger and more uniform interaction of FPS with the target, with a minimum of FIB damage. This paper presents the convergence of experimental and numerical results in establishing the concept of the Slow Focus Mode in kJ machines as an advantageous operational mode for working on the surface of materials. Clearly further studies are needed to more comprehensively understand and explain the complex interaction of fusion plasmas with walls beyond the simple picture that may be portrayed by invoking any one parameters such as the damage factor. (We thank the Reviewer for stressing this.)

Acknowledgment

We acknowledge research grants INT-CPR-01-02-2012 and FRGS/2/2013/SG02/INTI/01/1.

References

[1] IAEA-TECDOC-1708, Integrated Approach to Dense Magnetized Plasmas Applications in Nuclear Fusion Technology, International Atomic Energy Agency (IAEA), Vienna, 2013.
[2] Vladimir A. Gribkov, Artur Malaquias, Dense magnetized plasma and its applications: review of the 3-year activity of the IAEA Co-ordinated research programme, Nukleonika 51 (1) (2006) 5–13.
[3] Sh Al-Hawat, M. Soukieh, M. Abou Kharoub, W. Al-Sadat, Using Mather-type plasma focus device for surface odification of AISI304 Steel, Vacuum 8 (4) (2009) 907–912.
[4] M. Hassan, R. Ahmad, A. Qayyum, G. Murtaza, A. Waheed, M. Zakaullah, Surface Modification of $AlFe_{1.8}Zn_{0.8}$ Alloy by Using Dense Plasma Focus, vol. 81, (2006), pp. 291–298 no. 3.
[5] V. Damideh, et al., Design and construction of the 5 kJ filippov-type plasma focus with brass anode, J. Fusion Energy 30 (6) (2011) 462–465.
[6] V. Damideh, et al., Design and fabrication of 11.2 kJ mather-type plasma focus IR-MPF-1 with high drive parameter, J. Fusion Energy 31 (1) (2011) 47–51.
[7] V.A. Gribkov, et al., In-line and following-up tests of perspective fusion-reactor materials in plasma focus devices, Czech. J. Phys. 56 (12) (2006) 1401–1416.
[8] R.S. Rawat, High-energy-density pinch plasma: a unique non-conventional tool for plasma nanotechnology, IEEE Trans. Plasma Sci. 41 (4) (2013) 701–715.
[9] A. Bernard, et al., Scientific status of plasma focus research, J. Mosc Phys. Soc. 8 (2) (1998) 93–170.
[10] S.H. Saw, V. Damideh, P.L. Chong, P. Lee, R.S. Rawat, S. Lee, A 160 kJ dual plasma focus (DuPF) for fusion-relevant materials testing and nano-materials fabrication, Int. J. Mod. Phys.: Conference SeriesVol. 32 (2014) 1460322.
[11] S. Lee, S.H. Saw, The slow focus mode in plasma focus for fast plasma stream nano-materials fabrication: selection of energy of bombarding particles by pressure control, Journal of Science, Engineering and Technology 10 (2) (2014) 17–23.
[12] B.J. Chan, Four-chord Interferometer Measurements of the ZaP Flow Z-Pinch, University of Washington, Washington, 2008.
[13] S.H. Saw, P. Lee, R.S. Rawat, R. Verma, D. Subedi, R. Khanal, P. Gautam, R. Shrestha, A. Singh, S. Lee, Comparison of measured neutron yield versus pressure curves for FMPF-3, NX2 and NX3 plasma focus machines against computed results using the lee model code, J. Fusion Energy 34 (3) (2015) 474–479.
[14] A. Schmidt, V. Tang, D. Welch, Fully kinetic simulations of dense plasma focus Z-pinch devices, Phys. Rev. Lett. 109 (2012) 20500.
[15] M. Krishnan, The dense plasma focus: a versatile dense pinch for diverse applications, Plasma Science, IEEE Transactions on 40 (12) (2012) 3189–3221.
[16] D.E. Potter, Numerical studies of the plasma focus, Phys. Fluids 14 (9) (1971) 1911–1924.
[17] José H. González, Alejandro Clausse, Horacio Bruzzone, Pablo C. Florido, A lumped parameter model of plasma focus, Plasma Science, IEEE Transactions on 32 (3) (2004) 1383–1391.
[18] S. Lee, "Radiation in plasmas", vol II, ed. by B. McNamara, Proceedings of Spring College in Plasma Physics 1983, ICTP, Trieste, (World Scientific Pub Co, Singapore, 1984, pp. 978–987 ISBN 9971-966-37-9.
[19] Laser and plasma technology, in: S. Lee, B.C. Tan, C.S. Wong, A.C. Chew (Eds.), Proceedings of First Tropical College on Applied Physics 26th Dec 1983–14th Jan 1984, World Scientific Publishing Co., Kuala Lumpur, 1985, pp. 38–62 ISBN 9971-

978-27-X.
[20] S. Lee, Radiative dense plasma focus computation package: RADPF, [Online]. Available: http://www.plasmafocus.net, (2015) http://www.intimal.edu.my/school/fas/UFLF.
[21] S. Lee, Plasma focus radiative model: review of the lee model code, J. Fusion Energy 33 (4) (2014) 319–335.
[22] M. Rosenbluth, R.K.M. Landshoff (Ed.), Magnetohydrodynamics, Stanford University Press, 1957, p. p57.
[23] D. Potter, The formation of high-density z-pinches, Nucl. Fusion 18 (6) (1978) 813.
[24] A. Mohamed, Abd Al-Halim, Estimation of the plasma sheath thickness and particle number density in the axial phase of plasma coaxial accelerator, Vacuum 138 (2017) 80–86.
[25] S. Lee, S.H. Saw, Pinch current limitation effect in plasma focus, Appl. Phys. Lett. 92 (2008) 1–3 021503.
[26] S. Lee, Current and neutron scaling for megajoule plasma focus machines, Plasma Phys. Contr. Fusion 50 (10) (2008).
[27] S. Lee, S.H. Saw, Jalil Ali, Numerical experiments on radiative cooling and collapse in plasma focus operated in krypton, J. Fusion Energy 32 (1) (2012) 42–49.
[28] S.H. Saw, et al., SXR measurements in INTI PF operated in neon to identify typical (normal N) profile for shots with good yield, Transactions on Plasma Science, IEEE, 2013.
[29] S.H. Saw, P.C.K. Lee, R.S. Rawat, S. Lee, Optimizing UNU/ICTP PFF plasma focus for neon soft X-ray operation, IEEE Trans. Plasma Sci. 37 (7) (2009) 1276–1282.
[30] S. Lee, Neutron yield saturation in plasma focus: a fundamental cause, Appl. Phys. Lett. 95 (2009) 151503.
[31] S.H. Saw, S. Lee, Scaling laws for plasma focus machines from numerical experiments, Energy Power Eng. (2010) 65–72.
[32] S. Lee, S.H. Saw, Plasma Focus Ion Beam Fluence and Flux –Scaling with Stored Energy 19 (2012) 112703.
[33] S. Lee, S.H. Saw, P.C.K. Lee, R.S. Rawat, H. Schmidt, Computing plasma focus pinch current from total current measurement, Appl. Phys. Lett. 92 (2008) 111501.
[34] Sing Lee, Serban Adrian, Dimensions and lifetime of the plasma focus pinch, IEEE Trans. Plasma Sci. 24 (3) (1996) 1101–1105.
[35] S. Lee, S.H. Saw, Plasma focus ion beam fluence and flux –for various gases, Phys. Plasmas 20 (2013) 062702.
[36] L. Soto, C. Pavez, J. Moreno, M.J. Inestrosa-Izurieta, F. Veloso, G. Gutierrez, J. Vergara, A. Clausse, H. Bruzzone, F. Castillo, L.F. Delgado-Aparicio, Phys. Plasmas 21 (2014) 122703.
[37] M. Akel, S. Alsheikh Salo, Sh Ismael, S.H. Saw, S. Lee, J. Fusion Energy 35 (4) (2016) 694–701.
[38] M. Hassan, et al., J. Phys. D Appl. Phys. 40 (2007) 769.
[39] S.R. Mohanty, et al., Jpn. J. Appl. Phys. 46 (2007) 3039.
[40] M. Akel, S. Alsheikh Salo, Sh Ismael, S.H. Saw, S. Lee, Comparison of measured and computed beam ion current densities emitted from two 2 kJ plasma focus machines, Vacuum 136 (2017) 163–167.
[41] Sh Al-Hawat, M. Akel, S. Lee, S.H. Saw, Model parameters versus gas pressure in two different plasma focus devices operated in argon and neon, J. Fusion Energy 31 (1) (2012) 13–20.
[42] Leopoldo Soto, Cristian Pavez, Jose Moreno, Marıa Jose Inestrosa-Izurieta, Felipe Veloso, Gonzalo Gutierrez, Julio Vergara, Alejandro Clausse, Horacio Bruzzone, Fermın Castillo, F. Luis, Delgado-Aparicio, Phys. Plasma. 21 (2014) 122703.
[43] S.H. Saw, V. Damideh, Jalil Ali, R.S. Rawat, P. Lee, S. Lee, Damage study of irradiated tungsten using fast focus mode of a 2.2 kJ plasma focus, Vacuum 144 (2017) 14–20.
[44] V. Damideh, J. Ali, S.H. Saw, R.S. Rawat, P. Lee, K.T. Chaudhary, Z.H. Rizvi, Shadab Dabagh, Fairuz Diyana Ismail, Sing Lee, Fast Faraday cup for fast ion beam TOF measurements in deuterium filled plasma focus device and correlation with Lee model, Phys. Plasmas 24 (6) (2017) 063302.